Percolation thresholds of randomly rotating patchy particles on Archimedean lattices

Quancheng Wang,[1] Zhenfang He,[1] Junfeng Wang,[2] and Hao Hu[1,*]
[1]*School of Physics and Optoelectronic Engineering, Anhui University, Hefei, Anhui 230601, China*
[2]*School of Physics, Hefei University of Technology, Hefei, Anhui 230009, China*

(Received 29 November 2021; accepted 24 February 2022; published 15 March 2022; corrected 24 March 2022)

We study the percolation of randomly rotating patchy particles on 11 Archimedean lattices in two dimensions. Each vertex of the lattice is occupied by a particle, and in each model the patch size and number are monodisperse. When there are more than one patches on the surface of a particle, they are symmetrically decorated. As the proportion χ of the particle surface covered by the patches increases, the clusters connected by the patches grow and the system percolates at the threshold χ_c. We combine Monte Carlo simulations and the critical polynomial method to give precise estimates of χ_c for disks with one to six patches and spheres with one to two patches on the 11 lattices. For one-patch particles, we find that the order of χ_c values for particles on different lattices is the same as that of threshold values p_c for site percolation on these lattices, which implies that χ_c for one-patch particles mainly depends on the geometry of lattices. For particles with more patches, symmetry becomes very important in determining χ_c. With the estimates of χ_c for disks with one to six patches, using analyses related to symmetry, we are able to give precise values of χ_c for disks with an arbitrary number of patches on all 11 lattices. The following rules are found for patchy disks on each of these lattices: (1) as the number of patches n increases, values of χ_c repeat in a periodic way, with the period n_0 determined by the symmetry of the lattice; (2) when mod $(n, n_0) = 0$, the minimum threshold value $\chi_{\min}$ appears, and the model is equivalent to site percolation with $\chi_{\min} = p_c$; and (3) disks with mod $(n, n_0) = m$ and $n_0 - m$ $(m < n_0/2)$ share the same χ_c value. The results can be useful references for studying the connectivity of patchy particles on two-dimensional lattices at finite temperatures.

DOI: 10.1103/PhysRevE.105.034118

I. INTRODUCTION

Patchy particles [1,2] are created by modifying the surface of colloidal particles, where each modified area is regarded as a patch. One-patch particles with two distinct surface areas are usually called Janus particles, and two-patch particles are called triblock Janus particles. These particles can be designed in various shapes, e.g., spheres, dumbbells, disks, and rods, and the patches can be decorated with different properties, e.g., chemical, optical, electrical, and magnetic properties. As model systems with anisotropic interactions, patchy particles are used to study equilibrium gels and water [3,4], and they can self-assemble into open lattices [5–7] such as the entropy-stabilized kagome lattice [5,6]. In two dimensions, systems of self-assembled rigid rods (particles with two narrow patches) exhibit continuous isotropic-nematic phase transitions on different lattices, which have been extensively studied [8–15]. When patchy disks or spheres are compressed tightly in two dimensions, they form a triangular lattice. Putting Janus particles onto the densely packed triangular lattice, various continuous thermodynamic phase transitions and critical phenomena have recently been observed [16–18].

Percolation is extensively studied in stochastic processes, phase transitions, and critical phenomena, and widely applied in various problems such as exploring gelation in polymers, transport behaviors in porous media, the spread of epidemics, the fractal structure of landscapes, etc. [19,20] There exist many studies on percolation of patchy particles in the continuum space, for which recent examples include different percolated states in mixtures of patchy colloids [21], reentrant percolation of inverse patchy colloids [22] and of patchy colloids on patterned substrates [23], effects of surface heterogeneity on percolation thresholds of random patchy spheres [24], and the design of patchy particle gels with tunable percolation thresholds [25]. However, except for a study on directed percolation of patchy disks on the square lattice [26], we find that the percolation behavior of patchy particles on lattices remains largely unexplored.

In this work, we study percolation of patchy particles on different lattices to fill the above gap. As model systems, we assume that each vertex of the lattice is occupied by a patchy particle, and that particles rotate randomly (in other words, the systems are with full lattice occupancy and at the infinite temperature). Two adjacent particles are considered as connected only when their patches are in contact with each other. As the proportion χ of the particle surface occupied by the patch(es) increases, the clusters formed by connected particles will gradually become larger. At a threshold value χ_c, a cluster that spans the entire lattice first forms, i.e., the percolation transition occurs. The threshold is an important parameter for percolation [19,20]; e.g., its dependence on concentration and temperature was explored in the 1980s in experimental and theoretical studies of the conductivity in

*Corresponding author: huhao@ahu.edu.cn

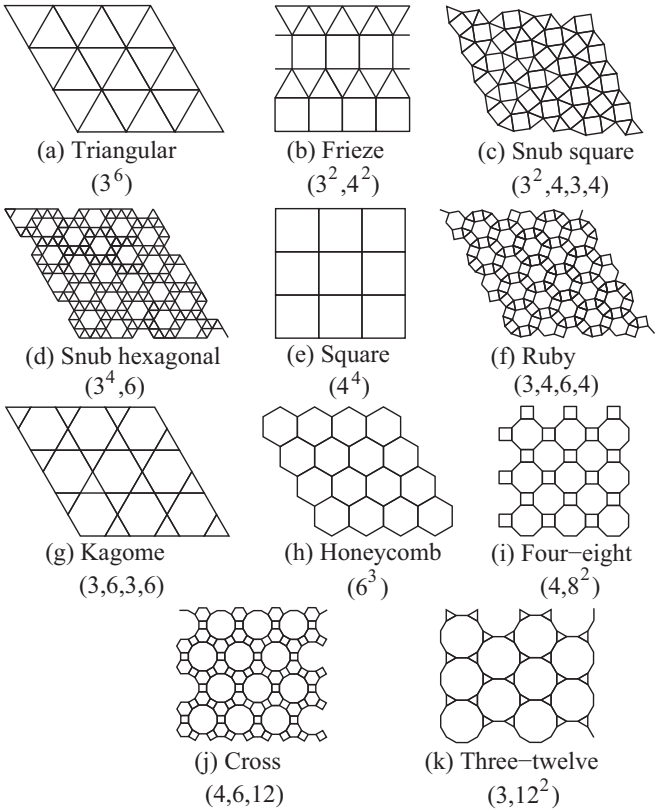

FIG. 1. The 11 Archimedean lattices in two dimensions. For each lattice, all vertices are equivalent if the lattice size is infinite or the boundary conditions are periodic. Lattice names are used as in Ref. [37], and under the names symbols are designated using the general notation proposed by Grünbaum and Shephard [39]. A brief introduction of the history and nomenclature of the lattices are available in Ref. [40].

interacting microemulsions [27], and it was recently used to predict a series of structural changes in compressed SiO_2 glasses [28]. Thus we focus on determining the χ_c values and exploring the dependence of these values on the symmetry and geometry of patchy particles and lattices. The results can provide references for further studies of patchy particles on two-dimensional (2D) lattices, such as exploring the connectivity of particles at finite temperatures and its relation to phase behaviors [8–18].

For the purpose above, we first numerically study disks with one to six patches and spheres with one to two patches, on all 11 Archimedean lattices in two dimensions, which are shown in Fig. 1. When there are more than one patches on a particle, the patches locate symmetrically and share the same size, as shown for patchy disks in Fig. 2. Monte Carlo (MC) simulations are conducted to produce independent configurations, and the recently developed critical polynomial method [29–38] is combined with MC sampling to precisely estimate χ_c of these models. For one-patch particles, it is found that the order of χ_c values on different Archimedean lattices is the same as that of threshold values p_c for site percolation on these lattices. This suggests that, for one-patch particles, the lattice geometry is the most important factor which affects χ_c values. For particles with more patches, their

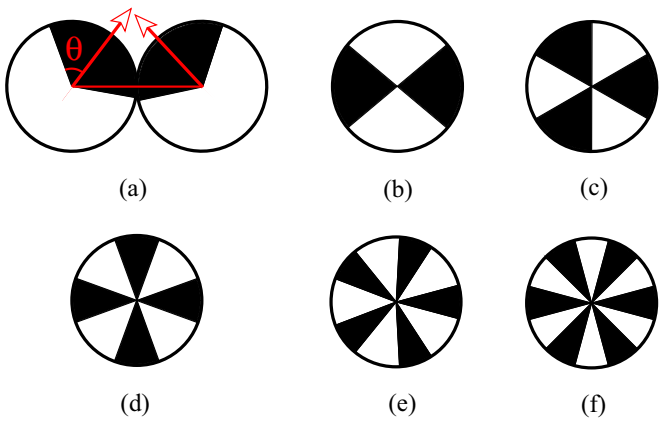

FIG. 2. Schematic drawings of patchy disks. On each disk the dark areas are patches, which share the same size and locate symmetrically when their number is more than one. The half-angle θ characterizes the size of a patch. Panels (a)–(f) show particles containing one to six patches, respectively. Panel (a) also exemplifies the connection of two particles, i.e., they are considered as connected if their patches touch each other. The red arrow indicates the direction of the particle, which is drawn by connecting the center of the particle and that of one patch.

χ_c values on different lattices do not follow the same order as those for one-patch particles, which reflects that symmetry significantly influence percolation thresholds of particles with more than one patches.

The role of symmetry in determining the χ_c values is further exhibited in analytic calculations of the probabilities of different patch-covering structures of a particle near the above numerically estimated values of χ_c. These calculations lead to expressions of the probabilities as a function of χ, which allow us to prove the equality of χ_c values for various models or explain the difference between close χ_c values for distinct models. As results, we are able to give precise values of χ_c for disks with an arbitrary number of patches on all 11 Archimedean lattices in two dimensions. We find that χ_c values for patchy disks on each of the lattices are governed by the following rules: (1) χ_c values repeat in a periodic way as the number of patches n increases, with the period n_0 determined by the symmetry of the lattice; (2) the minimum threshold value $\chi_{\min}$ appears when $\mod(n, n_0) = 0$, for which the model of patchy disks is equivalent to site percolation with $\chi_{\min} = p_c$; and (3) disks with $\mod(n, n_0) = m$ and $n_0 - m$ ($m < n_0/2$) share the same value of χ_c.

The remainder of this paper is organized as follows. Section II introduces the models and numerical methods. Section III presents our main results. A brief conclusion and discussion are given in Sec. IV. More details can be found in the Supplemental Material [41].

II. MODELS AND NUMERICAL METHODS

A. Models

For the Archimedean lattices, all vertices are equivalent and the lengths of edges are equal, as shown in Fig. 1. For the model of a given type of patchy particles on one of the Archimedean lattices, each vertex of the lattice is occupied

by a randomly rotating particle. The particle center is located right at the vertex, and its diameter is set equal to the edge length of the lattice; thus two particles at the ends of an edge are in contact with each other. Two neighboring particles are connected if one patch on one particle touches another patch on the other particle (the two patches both cover the same edge). As shown in Fig. 2(a), the size of a patch is characterized by the half-angle θ. The one- and two-patch spheres can be drawn similar to Figs. 2(a) and 2(b), except that a patch is a sphere cap with θ being the polar angle. For convenience of comparing thresholds of different types of particles, we also define the size of patches by the proportion χ of the particle surface covered by the patches, which is related to θ as

$$\chi = 2n\theta/2\pi = n\theta/\pi \tag{1}$$

for patchy disks, and as

$$\chi = \frac{n}{4\pi}\int_0^{\theta}\sin\theta d\theta\int_0^{2\pi}d\phi = n(1-\cos\theta)/2 \tag{2}$$

for patchy spheres. Here n is the number of symmetrically distributed patches on a particle. In experiments, the patch size can be designed through surface modification or compartmentalization [1,2].

B. The critical polynomial

The critical polynomial method is a powerful method proposed and developed in recent years to calculate percolation thresholds in two dimensions [29–38]. It originated from the fact that every exactly solved percolation threshold in two dimensions can be expressed as the unique root of a polynomial. For general (solved and unsolved) percolation models in two dimensions, the critical polynomial was first defined using a linearity hypothesis and symmetry analyses [29–31]. Then the recursive deletion-contraction algorithm [32] was proposed to find the polynomial. The latest developments of the method are the alternative probabilistic, geometrical interpretation of the critical polynomial [33] and transfer-matrix techniques for its calculation [34–37]. Unprecedented estimates for thresholds of unsolved planar-lattice models have been obtained; e.g., for bond percolation on the kagome lattice, the precision of the estimate is in the order of 10^{-17} [37]. The critical polynomial has also been combined with MC sampling to provide high-precision estimates of threshold values, e.g., for nonplanar and continuum percolation models [38], for which transfer-matrix calculations are difficult.

For a finite periodic lattice B in two dimensions, the probabilistic, geometrical definition of the critical polynomial [33] is

$$P_B \equiv R_2 - R_0. \tag{3}$$

Here R represents the wrapping (or crossing) probability [42–44], where "wrapping" means that, when putting the periodic lattice in two dimensions onto a torus, there exists a percolation cluster which wraps around the torus. The quantity R_2 is the probability of wrapping in two directions, and R_0 is the probability of nonwrapping. If filling the infinite space in two dimensions using copies of B in some periodic way, wrapping in two directions means that there is an open cluster which connects every copy, and nonwrapping means that no infinite copies of B can be connected by open clusters [33].

Due to universality [33], the root $p(L)$ of $P_B(p, L) = 0$ gives an estimate of the percolation threshold that becomes more accurate as the linear size L of the lattice B is increased. Here p represents the control parameter for the percolation problem, e.g., the occupation probability ($p \in [0, 1]$) for bond or site percolation. From previous studies on the critical polynomial [29–37], it is known that $p(L) = p_c$ [$p_c \equiv p(L \to \infty)$] for exactly solved lattice models, even at the smallest L, and that, for unsolved percolation problems, $p(L)$ very quickly approaches p_c as L increases. For example, on Archimedean lattices, the unsolved bond percolation thresholds behave as $[p(L) - p_c] \simeq \sum_{k=1}^{\infty} A_k L^{-\Delta_k}$, with $\Delta_1 = 4$ or 6, and $\Delta_i > \Delta_j$ when $i > j$ [37]. The finite-size correction of P_B is much smaller than that for other quantities such as wrapping probabilities [38].

The critical polynomial P_B is a dimensionless quantity, since $P_B(p_c, L \to \infty) = 0$. Thus in the renormalization group formulation [45], P_B has the finite-size scaling formula [38]

$$P_B(t, u_1, u_2, L) = P_B(L^{y_t}t, L^{y_1}u_1, L^{y_2}u_2). \tag{4}$$

Here $t \propto p - p_c$ is the relevant thermal renormalization scaling field, and $y_t = 1/\nu = 3/4$ is the associated renomalization exponent. The parameters u_1 and u_2 represent two leading irrelevant scaling fields with renormalization exponents $y_2 < y_1 < 0$. When assuming $y_2 > 2y_1$, by Taylor expansion to the first order, one gets

$$P_B(p, L) \simeq a_1(p - p_c)L^{y_t} + b_1L^{y_1} + b_2L^{y_2}, \tag{5}$$

where a_1, b_1, and b_2 are nonuniversal amplitudes. The irrelevant exponents are related to Δ values as $y_1 = y_t - \Delta_1$ and $y_2 = y_t - \Delta_2$ [38]. Our MC data will be fitted by the above finite-size scaling formula, with p replaced by θ, though the irrelevant exponents may be different from those of bond percolation on Archimedean lattices [37].

C. Monte Carlo simulation

The MC method is used to sample independent configurations for 88 models, including six types of patchy disks and two types of patchy spheres, on all 11 Archimedean lattices in two dimensions. For a single configuration, a random direction is generated for each particle to simulate the random rotation. In simulations, each lattice is encoded with the aid of a square or triangular array, whose correspondence with the actual lattice is shown in Figs. S1–S11 [41], and periodic boundary conditions are employed for the lattices. The number of vertices (equivalent to the number of particles) on each lattice can be calculated from L, as shown in Table S1 [41]. Hereafter L is the linear size of the square or triangular array for encoding the lattices, which is in proportion to the actual linear size. We conduct simulations at different patch sizes and systems sizes, and use sampled values of P_B to determine the percolation threshold θ_c (χ_c).

In our MC simulations, we simulated systems with up to $O(10^5)$ particles. At least 10^8 independent configurations were generated for each set of (θ, L) values, for all 88 models (up to 10^{10} independent configurations for one-patch disks when $L < 16$, as shown in Table S2 [41]). The total simulation

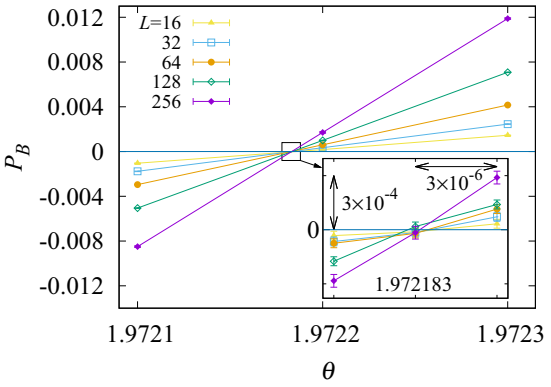

FIG. 3. Plot of P_B vs θ for one-patch disks on triangular lattices for different linear sizes L. The lines are added to guide the eye.

time was about 14.6 months if using a computer workstation with 2 Intel Xeon Scalable Gold 6130 CPU and 8 × 16 GB DDR4 ECC Registered Shared Memory (time for each model is shown in Table S3 [41]).

III. RESULTS

We first present numerical results for one-patch particles, then for particles with two to six patches. Precise estimates of χ_c for these particles on 11 Archimedean lattices are obtained by combining MC simulations and the critical polynomial method. It is found that the lattice geometry mainly determines χ_c for one-patch particles, and that the symmetry of patches and lattices significantly affects χ_c for particles with more patches. Furthermore, with the above numerical estimates of χ_c, using analyses related to symmetry, we give values of χ_c for disks with an arbitrary number of patches on all 11 Archimedean lattices. We also present the rules governing χ_c values of patchy disks on these lattices.

A. Numerical results for one-patch particles

1. One-patch disks

For one-patch disks on the triangular lattice, the plot of P_B vs θ is shown in Fig. 3. It can be seen that curves for different sizes approximately cross near $\theta_c \simeq 1.972\,183$. To more precisely estimate the percolation threshold θ_c, we use Eq. (5), with p replaced by θ, to fit the data of P_B according to the least-square criterion. When performing the fits, we gradually increase $L_{\min}$ and exclude data points for $L < L_{\min}$. In general, the fit results are acceptable only when χ^2 is less than or close to the degree of freedom (DOF), and the decrease

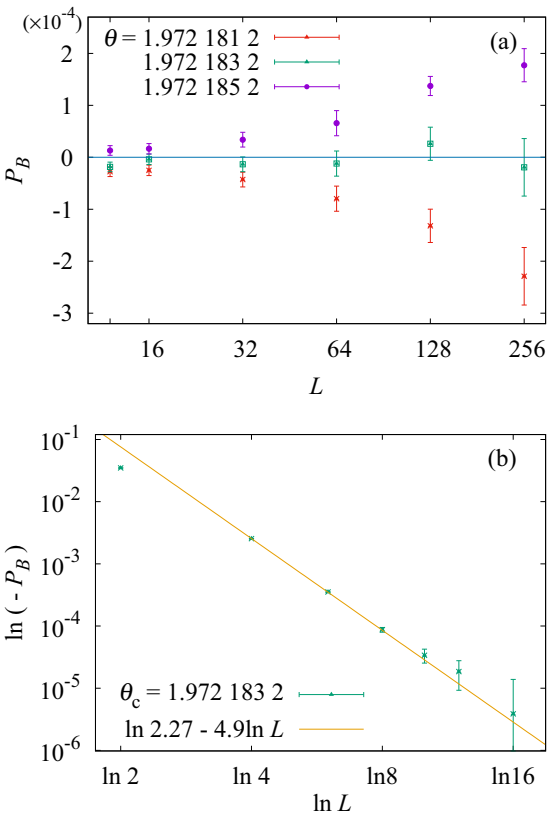

FIG. 4. Plots for one-patch disks on the triangular lattice: (a) P_B vs L at $\theta_c = 1.972\,183\,2$ and two nearby values of θ. As θ deviates from θ_c, the curves bend upwards ($\theta > \theta_c$) or downwards ($\theta < \theta_c$). (b) $\ln(-P_B)$ vs $\ln L$ at θ_c for small sizes L. The slope of the straight line is given by the correction exponent $y_1 \simeq -4.9$.

of χ^2 per DOF does not exceed one when increasing $L_{\min}$. Fits are made with fixed $y_t = 3/4$, and the results are shown in Table I. When setting $b_2 = 0$, the fit results show that the leading irrelevant exponent is $y_1 \simeq -4.9$. When y_2 is fixed at -6, -7, or -8, the fit results are also consistent with $y_1 \simeq -4.9$. Thus we put our final estimate as $y_1 = -4.9(3)$. From Table I, the percolation threshold of one-patch disks on the triangular lattice is estimated to be $\theta_c = 1.972\,183\,20(8)$, i.e., $\chi_c = 0.627\,765\,41(3)$. All error bars of quantities in this work can be regarded as $1\,\sigma$.

To demonstrate the above estimates of θ_c, we plot in Fig. 4(a) P_B vs L at θ_c and two nearby values. It can be seen that when θ deviates from θ_c, the curves bend upwards ($\theta > \theta_c$) or downwards ($\theta < \theta_c$) as the size L increases. Since

TABLE I. Fit results of the critical polynomial P_B for one-patch disks on the triangular lattice.

$L_{\min}$	χ^2/DOF	θ_c	a_1	b_1	y_1	b_2	y_2
6	63.6/79	1.972 183 20(7)	−1.65(4)	−2.1(6)	−4.9(2)		
8	62.6/76	1.972 183 20(7)	−1.65(4)	−2.2(30)	−4.9(6)		
4	83.8/88	1.972 183 20(7)	−1.65(4)	−2.2(25)	−4.9(4)	0.3(53)	−6
2	84.8/91	1.972 183 21(7)	−1.65(4)	−3.7(2)	−5.11(4)	9.2(5)	−7
4	83.8/88	1.972 183 20(7)	−1.65(4)	−2.2(13)	−4.9(3)	0.5(85)	−7
2	84.3/91	1.972 183 21(7)	−1.65(4)	−2.7(1)	−4.97(3)	13.0(6)	−8

TABLE II. Percolation thresholds χ_c of patchy particles on Archimedean lattices. The site-percolation thresholds p_c for these lattices are also included for comparison.

	Lattice	Triangular	Frieze	Snub square	Snub hexagonal
Disk	One-patch	0.627 765 41(3)	0.672 338 8(1)	0.672 346 35(4)	0.688 526 01(4)
	Two-patch	0.554 469 9(4)	0.624 383 7(6)	0.622 832 9(4)	0.625 385 2(6)
	Three-patch	0.558 806 6(7)	0.623 505 (1)	0.620 411 9(5)	0.617 753 2(7)
	Four-patch	0.554 469 2(4)	0.645 671 6(5)	0.670 484 3(5)	0.625 384 5(6)
	Five-patch	0.627 765 6(4)	0.658 762 8(6)	0.627 557 4(8)	0.688 525 6(5)
	Six-patch	0.500 000 1(5)	0.692 899 0(9)	0.756 361 (1)	0.579 497 9(9)
Sphere	One-patch	0.631 475 6(3)	0.676 869 4(4)	0.676 877 1(3)	0.694 042 7(3)
	Two-patch	0.532 379 5(7)	0.606 503 6(4)	0.605 554 2(5)	0.611 814 2(6)
p_c		1/2	0.550 213 (3) [40]	0.550 806 (3) [40]	0.579 498 (3) [40]
	Lattice	Square	Ruby	Kagome	Honeycomb
Disk	One-patch	0.713 444 50(3)	0.734 894 0(1)	0.745 229 66(5)	0.815 301 86(3)
	Two-patch	0.676 345 5(3)	0.717 490 7(3)	0.687 495 0(2)	0.815 301 6(3)
	Three-patch	0.713 444 6(3)	0.712 619 8(6)	0.725 743 3(6)	0.697 040 4(9)
	Four-patch	0.592 746 5(4)	0.775 605 0(8)	0.687 494 9(4)	0.815 301 9(3)
	Five-patch	0.713 444 4(8)	0.726 257 4(7)	0.745 229 4(8)	0.815 301 8(5)
	Six-patch	0.676 345 4(3)	0.764 013 5(7)	0.652 701 (2)	0.697 040 3(8)
Sphere	One-patch	0.718 297 8(6)	0.740 310 8(3)	0.753 481 7(3)	0.815 301 9(3)
	Two-patch	0.657 338 0(3)	0.706 489 1(8)	0.670 797 2(7)	0.806 134 8(4)
p_c		0.592 746 050 792 10(2) [35]	0.621 812 07(7) [34]	$1-2\sin(\pi/18)$ $= 0.652\,703\,644\ldots$ [46]	0.697 040 230(5) [34]
	Lattice	Four-eight	Cross	Three-twelve	
Disk	One-patch	0.827 011 22(3)	0.835 468 95(7)	0.859 494 83(5)	
	Two-patch	0.827 010 8(2)	0.835 469 0(4)	0.859 495 2(4)	
	Three-patch	0.815 649 0(4)	0.839 888 2(5)	0.859 495 3(5)	
	Four-patch	0.856 560 1(4)	0.865 225 2(7)	0.859 494 7(5)	
	Five-patch	0.815 649 6(4)	0.821 517 4(7)	0.843 143 7(8)	
	Six-patch	0.827 011 3(3)	0.839 888 4(5)	0.903 950 3(5)	
Sphere	One-patch	0.827 533 2(2)	0.835 822 4(4)	0.867 995 5(3)	
	Two-patch	0.818 019 5(4)	0.826 182 5(5)	0.852 055 5(5)	
p_c		0.729 723 2(5) [34]	0.747 800 2(2) [34]	$[1-2\sin(\pi/18)]^{1/2}$ $= 0.807\,900\,764\ldots$ [40]	

$P_B \simeq b_1 L^{y_1}$ at θ_c, the estimate of $y_1 \simeq -4.9$ is illustrated in Fig. 4(b) as the slope of the straight line.

For one-patch disks on other 10 Archimedean lattices, we also conduct similar analyses for the simulation data. Plots of P_B vs θ are shown in Fig. S12 [41]. Fits of the data also yield precise values of the percolation threshold χ_c for these lattices, as summarized in Table II. By observing the above χ_c values for one-patch disks on all 11 Archimedean lattices and p_c values for site percolation on these lattices, we find that the two sets of values follow the same order, as plotted in Fig. 5. The order can be regarded as from lattices with large coordination numbers to those with small coordination numbers, and when the coordination numbers are the same, it is from lattices with small variances of angles (around a vertex) to those with large variances. Thus, similar to p_c for site percolation, χ_c for one-patch disks on Archimedean lattices are mainly influenced by the lattice geometry.

The threshold values of one-patch disks on the frieze and snub square lattices are very close since the two lattices share the same coordination number and variance of angles. We find that their order can also be understood from geometry as follows. The patch of a disk can cover several neighboring edges connecting to the disk center, and various patch-covering structures occur with different probabilities, which can be obtained by analyzing the configurations as exemplified by the calculations for the frieze lattice in the Supplemental Material [41]. In Table III, we show these probabilities for patch sizes χ near χ_c of the two lattices. From the table, it is observed that three-edge patch covering occurs with same probabilities on the two lattices, as well as four-edge patch covering. However, for three-edge patch covering, the frieze lattice has a structure with two adjacent $\pi/2$ angles; and for four-edge covering, the frieze lattice has two structures (both occurring with probability $\chi - 2/3$) with two adjacent $\pi/2$ angles, while the snub square lattice has only one structure (occurring with probability $\chi - 2/3$) with two $\pi/2$ angles. Since structures with two adjacent $\pi/2$ angles are more open than other structures, the frieze lattice has a slightly lower percolation threshold than the snub square lattice, which is confirmed by our numerical estimates in Table II.

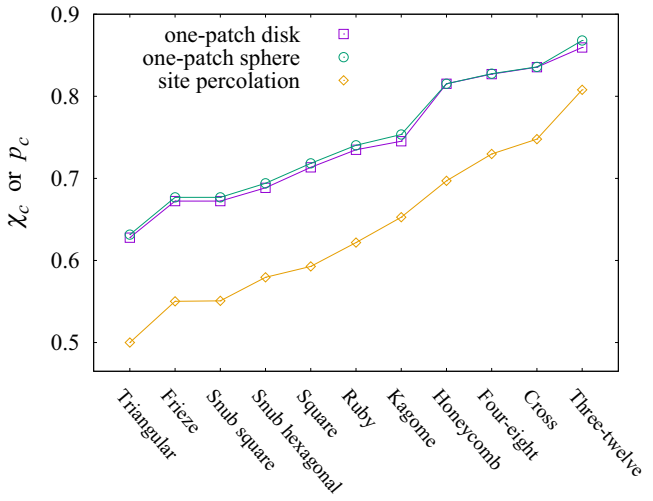

FIG. 5. Plots of percolation thresholds χ_c for one-patch disks and spheres, and p_c for site percolation. The values of the thresholds are summarized in Table II, where p_c values come from the cited references. The lines are added to guide the eye.

Besides χ_c, we also get estimates of the leading irrelevant exponent y_1 for one-patch disks on other Archimedean lattices. The results of y_1 are summarized in Table IV. For lattices whose values of y_1 are absent in the table, the finite corrections are also small, but the current data are not sufficient for determining y_1. The presented estimates of y_1 are close to $y_1 = y_t - \Delta_1 = -3.25$ or -5.25 for unsolved bond percolation models on Archimedean lattices [37]. Besides the triangular lattice, we also make plots of P_B vs L at the estimated thresholds for one-patch disks on other lattices, as shown in Fig. S20 [41], which demonstrate the scaling $P_B(\theta_c, L) \simeq b_1 L^{y_1}$ with the estimated values of y_1.

TABLE III. Probabilities of different patch-covering structures of a particle, for one-patch disks on the frieze and snub square lattices, as a function of χ near estimated χ_c of the two lattices. Bold lines indicate that corresponding edges are covered by the patch of a disk placed on the central vertex. Some details for calculating these probabilities are given in the Supplemental Material [41].

Lattice	Type	Structure	Probability	Probability Sum
Frieze	3-edge	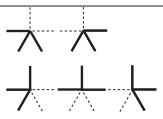	$2(3/4-\chi)$	$4-5\chi$
			$3(5/6-\chi)$	
	4-edge	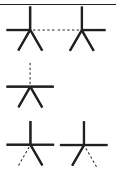	$2(\chi-7/12)$	$5\chi-3$
			$\chi-1/2$	
			$2(\chi-2/3)$	
Snub square	3-edge	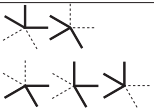	$2(3/4-\chi)$	$4-5\chi$
			$3(5/6-\chi)$	
	4-edge	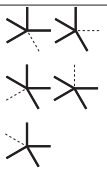	$2(\chi-7/12)$	$5\chi-3$
			$2(\chi-7/12)$	
			$\chi-2/3$	

TABLE IV. Results of y_1 from fitting the data of the critical polynomial P_B, for one-patch disks or spheres on different Archimedean lattices. Dashed entries indicate that the values cannot be determined with the current data.

Lattice	y_1(disk)	y_1(sphere)
Triangular	−4.9(3)	−3.1(1)
Frieze	−3.3(1)	−3.3(1)
Snub square	−3.7(1)	−3.9(1)
Snub hexagonal	—	—
Square	−3.3(4)	−3.5(2)
Ruby	—	—
Kagome	−5.2(4)	−5.4(1)
Honeycomb	−3.7(1)	−4.2(1)
Four-eight	−4.7(4)	−3.9(1)
Cross	—	—
Three-twelve	−3.1(2)	—

2. *One-patch spheres*

To observe the effect of particle shape on the percolation threshold, we also conduct simulations for one-patch spheres on Archimedean lattices. Similar analyses are performed for the simulation data. The resulting threshold values χ_c are also summarized in Table II and plotted in Fig. 5. It can be seen that, except on the honeycomb lattice, χ_c values for one-patch spheres are slightly larger than those for one-patch disks, and the calculated differences $[(\chi_c^{\text{sphere}} - \chi_c^{\text{disk}})/\chi_c^{\text{disk}}]$ are at most 1.1%. On the honeycomb lattice, within error bars, one-patch disks and spheres are found to share the same threshold. The thresholds χ_c for one-patch spheres on different lattices also follow the same order as that for one-patch disks, implying that for one-patch spheres χ_c are also mainly influenced by the lattice geometry.

We also get the estimates of y_1 for one-patch spheres on the lattices, as summarized in Table IV. The values of y_1 for one-patch spheres and disks are very close for most lattices. Plots of P_B vs θ or L for one-patch spheres are presented in Figs. S13 and S21 [41], which demonstrate our estimates of χ_c and y_1.

B. Numerical results for particles with two to six patches

We also conduct MC simulations for disks with two to six patches and spheres with two patches, on all 11 Archimedean lattices. Plots of P_B vs θ are shown in Figs. S14 to S19 [41], in which approximate intersections of lines for different sizes can be observed. By fitting the data of P_B near the intersection points, we also obtain precise percolation thresholds for these models, as summarized in Table II. These threshold values are plotted together with those for site percolation, as in Fig. 6.

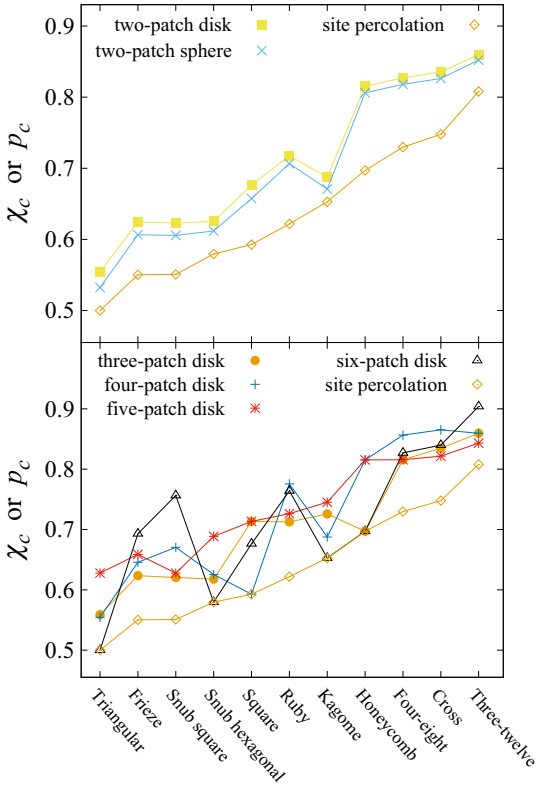

FIG. 6. Plots of percolation thresholds χ_c for particles with two to six patches, and p_c for site percolation, on 11 Archimedean lattices. The values of the thresholds are summarized in Table II, where p_c values come from the cited references. The lines are added to guide the eye.

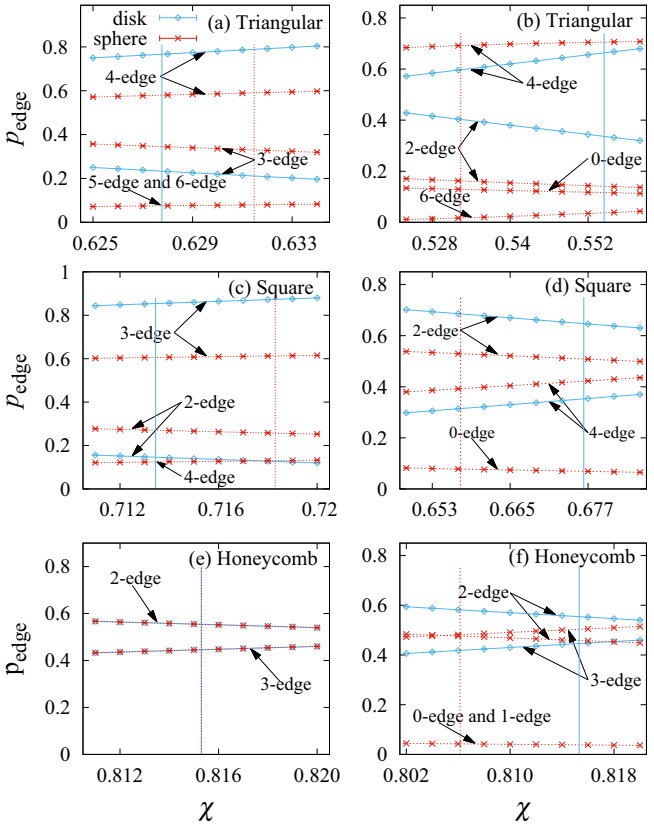

FIG. 7. Probabilities of different patch-covering structures p_{edge} of a particle for χ near χ_c, on the triangular, square, and honeycomb lattices. Plots (a), (c), and (e) are for one-patch particles, and plots (b), (d), and (f) are for two-patch particles. Vertical solid and dashed lines indicate values of χ_c for the disks and spheres, respectively. For one-patch disks and spheres on the honeycomb lattice, the probabilities are the same, which leads to the equality of χ_c for spheres and disks.

1. Two-patch particles

From plots for two-patch particles (disks or spheres) in Fig. 6, comparing with plots for one-patch particles in Fig. 5, an obvious feature is that the curves become nonmonotonic. The local minimum appears at the kagome lattice, for which the symmetry of the two triangles connected to a vertex matches the symmetry of the two patches on a particle. Thus symmetry become very important in determining χ_c values of two-patch particles.

From Table II, if one compares the χ_c values for two-patch particles with those for one-patch particles in more detail, it can be found that, while models of one-patch particles have slightly lower χ_c values on the frieze lattice than on the snub square lattice, models of two-patch particle have slightly higher χ_c values on the frieze lattice than on the snub square lattice. This can also be understood by calculating probabilities of different patch-covering structures of a particle, similar to calculations leading to Table III. For two-patch particles on the snub square lattice, the symmetry of two patches on the particle approximately matches the symmetry of two squares (or two triangles) connected to a vertex, which causes the χ_c value on the snub square lattice to be slightly lower than that on the frieze lattice.

In Sec. III A, for one-patch particles, it is found that differences of χ_c between disks and spheres are very small. However, for two-patch particles, in Fig. 6, it is seen that on most Archimedean lattices the differences of χ_c between disks and spheres are significantly larger than those for one-patch particles. And on a given lattice, while one-patch spheres have slightly higher χ_c than one-patch disks (except that on the honeycomb lattice one-patch disks and spheres share the same χ_c), two-patch spheres have lower χ_c than two-patch disks. Therefore, though not affecting the order of χ_c values for different lattices, the particle shape is still important in determining the values of χ_c.

To understand the change of χ_c values between one-patch and two-patch particles, for three regular lattices (triangular, square, and honeycomb), we plot the probabilities of different patch-covering structures of a particle for χ near χ_c, as in Fig. 7. From Figs. 7(a) and 7(c), it can be seen that, for one-patch particles, the lower value of χ_c for disks (comparing with that for spheres) is correlated with higher probabilities of large-edge patch-covering structures, e.g., four-edge and three-edge for the triangular and square lattices, respectively. From Figs. 7(b), 7(d), and 7(f), one also sees that, for two-patch particles, the lower value of χ_c for spheres (comparing with that for disks) is also correlated with higher probabilities of large-edge patch-covering structures, e.g., four- and six-edge for the triangular lattice, four-edge for the square lattice, and three-edge for the honeycomb lattice.

2. Three-to-six-patch disks

For disks with three to six patches, the role of symmetry is more explicitly exhibited. From Fig. 6, it can be seen that curves for these patchy particles are all nonmonotonic. Similar to that for two-patch particles at the kagome lattice, the local minimum of χ_c for four-patch disks at the kagome lattice and for five-patch disks at the snub square lattice can also be understood by the approximate matching of the symmetry of patches on a particle and the symmetry of the lattice. From Fig. 6 and Table II, it is interesting to find that χ_c values of some models are numerically equal to p_c values of site percolation on these lattices, such as three-patch disks on the honeycomb lattice, four-patch disks on the square lattice, and six-patch disks on the triangular, snub hexagonal, kagome, and honeycomb lattices. For each of these models, the symmetry of the patches on a particle perfectly matches the symmetry of the lattice, which leads to the fact that patches of a particle either cover all edges connected to the particle center with probability χ or cover no edge with probability $1-\chi$. Thus the models are exactly equivalent to the corresponding site percolation models with $\chi_c = p_c$. For other models considered, at $\chi = p_c$, the probability of an all-edge patch-covering structure is smaller than p_c, and other patch-covering structures lead to lower connection. Therefore, their χ_c values should be larger than p_c for site percolation on these lattices, which is supported by results in Table II and can be easily seen in Figs. 5 and 6.

From Table II, it is also interesting to see that, within error bars, χ_c of some different patchy particles on a given lattice share the same value. These include the following:

(1) On the triangular (or snub hexagonal, or kagome) lattice, χ_c of one- and five-patch disks, χ_c of two- and four-patch disks

(2) On the square lattice, χ_c of one-, three-, and five-patch disks, and χ_c of two- and six-patch disks

(3) On the honeycomb lattice, χ_c of one-, two-, four-, and five-patch disks and of one-patch spheres, and χ_c of three- and six-patch disks

(4) On the four-eight lattice, χ_c of one-, two-, and six-patch disks, and χ_c of three- and five-patch disks

(5) On the cross lattice, χ_c of one- and two-patch disks, and χ_c of three- and six-patch disks

(6) On the three-twelve lattice, χ_c of one- to four-patch disks.

The above equalities of χ_c values can be understood by calculating probabilities of different patch-covering structures of a particle for χ near χ_c. For example, on the honeycomb lattice, for one-patch spheres, it can be verified numerically that the patch-covering probabilities are equal to those for one-patch disks [e.g., see Fig. 7(e)]. For patchy disks, similar to results in Table III, using analytical calculations we can obtain the probabilities of different patch-covering structures of a particle as a function of χ near χ_c, as presented in the following section. Since percolation of patchy particles can be understood as connection of patch-covering structures of particles at the vertices, and there is only a single percolation threshold for a given model, the same expressions (as functions of χ) for these probabilities near χ_c can prove that these equalities of χ_c values hold exactly.

C. Results for disks with an arbitrary number of patches

In the previous subsection, it is found that several models of patchy disks are equivalent with site percolation on the lattices. This result can be generalized to disks with more patches: n-patch ($n > 0$) disks with $\mod(n, 3) = 0$ on the honeycomb lattice, with $\mod(n, 4) = 0$ on the square lattice, with $\mod(n, 6) = 0$ on the triangular, snub hexagonal, and kagome lattices, with $\mod(n, 8) = 0$ on the four-eight lattice, with $\mod(n, 12) = 0$ on the frieze, snub square, ruby, cross, and three-twelve lattices. These models are equivalent to site percolation since the patches on a disk either cover all edges connecting to the disk center with probability χ or cover no edge with probability $1-\chi$.

It is also found in previous subsections that several models of patchy disks can share the same χ_c value. Considering the above equivalences with site percolation, and observing these equalities of χ_c values [e.g. on the square lattice the equality of χ_c for disks with one (two) and five (six) patches], we wonder if χ_c values on a given lattice appear in a periodic way as the number of patches n increases, and if there is any other rule governing the χ_c values.

To explore possible periodic behaviors, we first try to calculate probabilities of different patch-covering structures of a disk as a function of χ for three regular lattices (honeycomb, square, and triangular), near previously estimated values of χ_c in Table II. Exemplary calculations for the triangular lattice and some calculation details for other two lattices are included in the Supplemental Material [41]. It is found that indeed there are periodic behaviors for these probabilities of different patch-covering structures, as summarized in Table V. As mentioned in the previous subsection, the same expressions as functions of χ for these probabilities near estimated χ_c prove that the equality of χ_c values holds exactly. Thus, from results in Table II, as the number of patches on a disk n increases, χ_c values appear with a period $n_0 = 3$, 4, and 6 for the honeycomb, square, and triangular lattices, respectively. Since the snub hexagonal and kagome lattices can be regarded as sublattices of the triangular lattice, we then calculate probabilities of different patch-covering structures of a disk on these two lattices by making use of the triangular lattice, as shown in Tables S5 and S6 [41]. The results for the snub hexagonal and kagome are also summarized in Table V, which confirm that on these two lattices χ_c values appear with a period $n_0 = 6$.

For calculating probabilities of different patch-covering structures of a patchy disk at a vertex of the four-eight lattice, we can first place the disk at the center of a regular octagon and consider the patch-covering of edges connecting the center and the vertices of the octagon, then use these intermediate results to get the final results. Some details are shown in Tables S7 and S8 [41], and the final results are also summarized in Table V, which shows that on the four-eight lattice χ_c values appear with a period $n_0 = 8$. Similarly, we can make use of the regular dodecagon to get probabilities of different patch-covering structures of a patchy disk at a vertex of other five Archimedean lattice in two dimensions. Some details for these calculations are included in Tables S9 to S23 [41]. Final results for these five lattices are summarized in Table VI, which prove that χ_c values on these lattices appear with a period $n_0 = 12$.

TABLE V. Probabilities of different patch-covering structures as a function of χ near χ_c, for n-patch disks on the honeycomb, square, triangular, snub hexagonal, kagome, and four-eight lattices. For each lattice, the last row shows estimates of percolation thresholds χ_c by combining numerical estimates in Table II. *Regarding two-edge structures on the kagome lattice, for n-patch disks with $\mathrm{mod}\ (n, 6) = 3$, the two edges have a $2\pi/3$ angle, while for disks with $\mathrm{mod}\ (n, 6) = 2$ or 4, the two edges are on the same straight line.

	Type	mod $(n, 3)$				
		1	2			
Honeycomb	Zero-edge					
	Two-edge	$3-3\chi$	$3-3\chi$			
	Three-edge	$3\chi-2$	$3\chi-2$			
	χ_c	0.815 301 8(3)	0.815 301 8(3)			
	Type	mod $(n, 4)$				
		1	2	3		
Square	Zero-edge					
	Two-edge	$3-4\chi$	$2-2\chi$	$3-4\chi$		
	Three-edge	$4\chi-2$		$4\chi-2$		
	Four-edge		$2\chi-1$			
	χ_c	0.713 444 5(4)	0.676 345 5(4)	0.713 444 5(4)		
	Type	mod $(n, 6)$				
		1	2	3	4	5
Triangular	Two-edge		$2-3\chi$		$2-3\chi$	
	Three-edge	$4-6\chi$		$2-2\chi$		$4-6\chi$
	Four-edge	$6\chi-3$	$3\chi-1$		$3\chi-1$	$6\chi-3$
	Six-edge			$2\chi-1$		
	χ_c	0.627 765 5(2)	0.554 469 6(4)	0.558 806 6(7)	0.554 469 6(4)	0.627 765 5(2)
	Type	mod $(n, 6)$				
		1	2	3	4	5
Snub hexagonal	One-edge		$2/3-\chi$		$2/3-\chi$	
	Two-edge		$4/3-2\chi$	$1-\chi$	$4/3-2\chi$	
	Three-edge	$10/3-4\chi$	$2\chi-2/3$	$1-\chi$	$2\chi-2/3$	$10/3-4\chi$
	Four-edge	$3\chi-5/3$	$\chi-1/3$		$\chi-1/3$	$3\chi-5/3$
	Five-edge	$\chi-2/3$		$2\chi-1$		$\chi-2/3$
	χ_c	0.688 525 8(3)	0.625 384 9(7)	0.617 753 2(7)	0.625 384 9(7)	0.688 525 8(3)
	Type	mod $(n, 6)$				
		1	2	3	4	5
Kagome	Two-edge	$5/3-2\chi$	$2-2\chi$	$(2-2\chi)^*$	$2-2\chi$	$5/3-2\chi$
	Three-edge	$2/3$				$2/3$
	Four-edge	$2\chi-4/3$	$2\chi-1$	$2\chi-1$	$2\chi-1$	$2\chi-4/3$
	χ_c	0.745 229 5(5)	0.687 494 9(4)	0.725 743 3(6)	0.687 494 9(4)	0.745 229 5(5)
	Type	mod $(n, 8)$				
		1 or 7	2 or 6	3 or 5	4	
Four-eight	One-edge			$7/4-2\chi$	$1-\chi$	
	Two-edge	$3-3\chi$	$3-3\chi$	$\chi-1/2$	$1-\chi$	
	Three-edge	$3\chi-2$	$3\chi-2$	$\chi-1/4$	$2\chi-1$	
	χ_c	0.827 011 0(1)	0.827 011 0(1)	0.815 649 3(4)	0.856 560 1(4)	

It should be noted that, for the lattices with periods $n_0 = 12$ and 8, when performing the calculations for probabilities of different patch-covering structures of a disk, we have made use of an assumed symmetry from observing expressions of other lattices. Namely, for the honeycomb, square, triangular, snub hexagonal, and kagome lattices, it is found that there is a symmetry between models with $\mathrm{mod}\ (n, n_0) = m$ $(0 < m < n_0/2)$ and $\mathrm{mod}\ (n, n_0) = n_0 - m$. Our results confirm that indeed this symmetry also holds for the lattices with $n_0 = 8$ and 12. This symmetry allows us to give the χ_c values

TABLE VI. Probabilities of different patch-covering structures as a function of χ near χ_c, for n-patch disks on the frieze, snub square, ruby, cross, and three-twelve lattices. For each lattice, the last row shows estimates of percolation thresholds χ_c by combining numerical estimates in Table II. *On the cross lattice, the one- and two-edge structures for n-patch disks with mod $(n, 12) = 4$ are different from those for disks with mod $(n, 12) = 3$ or 6.

	Type	mod $(n, 12)$ 1 or 11	2 or 10	3 or 9	4 or 8	5 or 7	6
Frieze	One-edge				$4/3 - 2\chi$	$4/3 - 2\chi$	$1 - \chi$
	Two-edge		$2 - 3\chi$	$3/2 - 2\chi$	$\chi - 1/3$	$\chi - 1/3$	
	Three-edge	$4 - 5\chi$	χ	$1/2$	$2/3 - \chi$	$1/6$	
	Four-edge	$5\chi - 3$	$2\chi - 1$	$\chi - 1/2$	$2\chi - 2/3$	$1/3$	$1 - \chi$
	Five-edge			$\chi - 1/2$		$\chi - 1/2$	$2\chi - 1$
	χ_c	0.672 338 8(1)	0.624 383 7(6)	0.623 505 (1)	0.645 671 6(5)	0.658 762 8(6)	0.692 899 0(9)
	Type	mod $(n, 12)$ 1 or 11	2 or 10	3 or 9	4 or 8	5 or 7	6
Snub square	Zero-edge					$2/3 - \chi$	
	One-edge					$1/6$	
	Two-edge		$2 - 3\chi$	$3/2 - 2\chi$		$1/6$	$1 - \chi$
	Three-edge	$4 - 5\chi$	χ	$1 - \chi$	$2 - 2\chi$	$1/6$	$1 - \chi$
	Four-edge	$5\chi - 3$	$2\chi - 1$	$3\chi - 3/2$	$1/3$	$1/6$	
	Five-edge				$2\chi - 4/3$	$\chi - 1/3$	$2\chi - 1$
	χ_c	0.672 346 35(4)	0.622 832 9(4)	0.620 411 9(5)	0.670 484 3(5)	0.627 557 4(8)	0.756 361 (1)
	Type	mod $(n, 12)$ 1 or 11	2 or 10	3 or 9	4 or 8	5 or 7	6
Ruby	One-edge			$3/2 - 2\chi$		$3/2 - 2\chi$	
	Two-edge	$7/3 - 3\chi$	$5/3 - 2\chi$	$\chi - 1/2$	$2 - 2\chi$	$\chi - 1/3$	$2 - 2\chi$
	Three-edge	$2\chi - 2/3$	$2/3$	$1/2$		$1/6$	
	Four-edge	$\chi - 2/3$	$2\chi - 4/3$	$\chi - 1/2$	$2\chi - 1$	$\chi - 1/3$	$2\chi - 1$
	χ_c	0.734 894 0(1)	0.717 490 7(3)	0.712 619 8(6)	0.775 605 0(8)	0.726 257 4(7)	0.764 013 5(7)
	Type	mod $(n, 12)$ 1 or 11	2 or 10	3 or 9	4 or 8	5 or 7	6
Cross	One-edge			$1 - \chi$	$(1 - \chi)^*$	$11/12 - \chi$	$1 - \chi$
	Two-edge	$3 - 3\chi$	$3 - 3\chi$	$1 - \chi$	$(1 - \chi)^*$	$7/6 - \chi$	$1 - \chi$
	Three-edge	$3\chi - 2$	$3\chi - 2$	$2\chi - 1$	$2\chi - 1$	$2\chi - 13/12$	$2\chi - 1$
	χ_c	0.835 469 0(2)	0.835 469 0(2)	0.839 888 3(5)	0.865 225 2(7)	0.821 517 4(7)	0.839 888 3(5)
	Type	mod $(n, 12)$ 1 or 11	2 or 10	3 or 9	4 or 8	5 or 7	6
Three-twelve	One-edge					$11/6 - 2\chi$	$1 - \chi$
	Two-edge	$3 - 3\chi$	$3 - 3\chi$	$3 - 3\chi$	$3 - 3\chi$	$1/6$	$1 - \chi$
	Three-edge	$3\chi - 2$	$3\chi - 2$	$3\chi - 2$	$3\chi - 2$	$2\chi - 1$	$2\chi - 1$
	χ_c	0.859 495 0(4)	0.859 495 0(4)	0.859 495 0(4)	0.859 495 0(4)	0.843 143 7(8)	0.903 950 3(5)

of patchy disks with mod $(n, n_0) > 6$, without performing additional numerical simulations. We have tried to understand this symmetry by observing the patch-covering structures and found that this symmetry is associated with some symmetries of the structures, as shown in Fig. S25 [41], but we do not have a simple explanation for why this symmetry exists.

We also note that, for a fixed value of j, when probabilities of j-edge patch covering are the same for different models, the detailed structures with j-edge patch covering still can be different. This can be clearly seen from Table III. Here, for Table V, on the kagome lattice, though probabilities of j-edge patch covering are the same for n-patch disks with mod $(n, 6) = 2$, 3, and 4, the detailed structures of two-edge patch covering for disks with mod $(n, 6) = 3$ are different from those with mod $(n, 6) = 2$ and 4. Since two-edge structures for disks with mod $(n, 6) = 2$ and 4 are more open than those for disks with mod $(n, 6) = 3$, the χ_c value of the latter is larger than that of the other two. Similarly, on the cross lattice, since the two-edge structures for disks with mod $(n, 12) = 3$ and 6 are more open than that for disks with mod $(n, 12) = 4$, the χ_c value of the latter is larger than that of the former two.

IV. CONCLUSION AND DISCUSSION

To summarize, we study in this work the percolation of patchy particles which are randomly rotating on 11 Archimedean lattices in two dimensions. We combine MC simulations with the recently developed critical polynomial method to give precise estimates of the threshold values χ_c for 88 models, including disks with one to six patches and spheres with one to two patches, on the 11 lattices. These estimates are summarized in Table II. For one-patch particles, it is found that χ_c values on different lattices follow the same order as p_c values for site percolation on these lattices, which implies that in this case χ_c is mainly influenced by the geometry of the lattices. When there are more symmetrically distributed patches on a particle, the symmetry of the patches plays an important role, in addition to the geometry of the lattices. The χ_c values on different lattices do not follow the same order as those for one-patch particles.

Furthermore, to explore the role of symmetry, we consider χ_c of disks with an arbitrary number ($n > 0$) of symmetrically distributed patches. By analyzing probabilities of different patch-covering structures of a patchy disk at a vertex as functions of χ near the above estimates of χ_c, we give χ_c values for these n-patch disks on all 11 Archimedean lattices in two dimensions. The χ_c values are plotted in Fig. 8, in which the following rules are summarized: (1) for a given lattice, χ_c values appear in a periodic way, with the period n_0 determined by the symmetry of the lattice. We find that $n_0 = 3$ for the honeycomb lattice, $n_0 = 4$ for the square lattice, $n_0 = 6$ for the triangular, snub hexagonal, and kagome lattices, $n_0 = 8$ for the four-eight lattice, and $n_0 = 12$ for the remaining five lattices. (2) The minimum threshold value $\chi_{\min}$ of a lattice presents when $\mod(n, n_0) = 0$. Actually, at this condition, the model is equivalent to site percolation on the same lattice, with $\chi_{\min}$ being equal to the site-percolation threshold p_c, whose value is given in Table II. (3) For each lattice, χ_c for $\mod(n, n_0) = m$ $(0 < m < n_0/2)$ is the same as that for $\mod(n, n_0) = n_0 - m$. In addition, we find that there exist other equalities between χ_c values, such as χ_c values of disks with $\mod(n, 8) = 1$ and 2 on the four-eight lattice, those of disks with $\mod(n, 12) = 1$ and 2 and of disks with $\mod(n, 12) = 3$ and 6, both on the cross lattice, and those of disks with $\mod(n, 12) = 1$, 2, 3, and 4 on the three-twelve lattice. The precise values of χ_c for n-patch disks with $\mod(n, n_0) \neq 0$ are summarized in Tables V and VI.

Precise values of χ_c for one- and two-patch spheres are also available in Table II. Comparing with one- and two-patch disks, our numerical results for the spheres suggest that changing the shape from disk to sphere does not affect the order of χ_c values for different lattices, but does affect the values of χ_c. It may be interesting to investigate χ_c of spheres with more patches, since more symmetries of patches are available on the sphere surface. As well, the current work can also be extended to other lattices. One example is the Lieb lattice in two dimensions. Percolation of four-patch disks on this lattice is equivalent to site percolation on the same lattice. Similar to the results in Sec. III B, this can be proved as the patches on a disk either cover all neighboring edges with probability χ or cover no edge with probability $1 - \chi$. Using MC simulations of site percolation and the critical polynomial method, we determine the threshold value as $\chi_c = p_c = 0.739\,706\,0(6)$ [41], which is much more precise than a recent estimate 0.739 6(5) [47]. It should be noted that site percolation on the Lieb lattice in two dimensions is equivalent to site-bond percolation on the square lattice with the same site and bond occupation probabilities, for which empirical formulas combined with the latest threshold values of both pure bond and pure site percolation lead to $p_c \simeq 0.742\,2$ [48] or $p_c \simeq 0.737\,6$ [49]. These values are quite close to our estimate above.

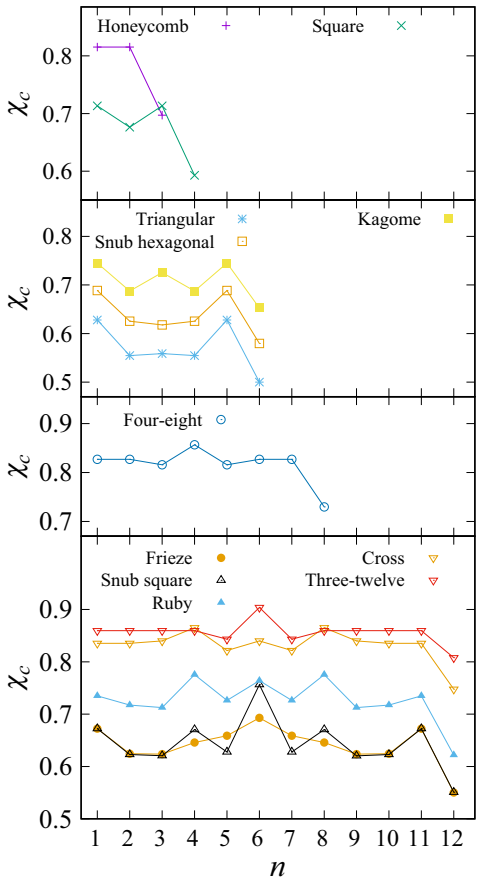

FIG. 8. The percolation threshold χ_c vs the number of patches on a disk n. As n increases, χ_c values appear in periodic ways, with the period being $n_0 = 3$ for the honeycomb lattice, $n_0 = 4$ for the square lattice, $n_0 = 6$ for the triangular, snub hexagonal, and kagome lattices, $n_0 = 8$ for the four-eight lattice, and $n_0 = 12$ for the remaining five lattices. For each lattice, the minimum threshold value $\chi_{\min}$ appears when $\mod(n, n_0) = 0$, and $\chi_{\min}$ is equal to the threshold p_c of site percolation on the same lattice. Moreover, χ_c for $\mod(n, n_0) = m$ $(0 < m < n_0/2)$ is the same as χ_c for $\mod(n, n_0) = n_0 - m$. Detailed values of χ_c (or p_c) can be read from Table II for $\mod(n, n_0) = 0$, and from Tables V and VI for $\mod(n, n_0) \neq 0$.

From the results in Table II and Sec. III C, it can be seen that, due to equivalences with site percolation, the thresholds of some models are exactly solvable, such as n-patch disks satisfying $\mod(n, 6) = 0$ on the triangular and kagome lattices, and satisfying $\mod(n, 12) = 0$ on the three-twelve lattice. One may wonder if there is any other patchy particle model whose percolation threshold can be exactly solved. For systems of rotating patchy particles, a bond is open if

patches on its two end particles contact, and the fact that a given bond is open affects the opening probabilities of neighboring bonds; thus one can regard these systems as correlated bond percolation. Taking this view, one can get an exactly solvable system by modifying the kagome lattice [50]. For the above rotating patchy particle system on the kagome lattice, one lets the bonds on each up-pointing triangle to be open according to the same contacting-patch rule as above, and declares the bonds on each down-pointing triangle to be open with probability one. Then bonds in each up-pointing triangle are correlated, but the up-pointing triangles are independent of each other. Thus from Ref. [50], the percolation threshold of this modified system can be exactly solved by the rule $P(A, B, C) = P(\overline{A}, \overline{B}, \overline{C})$, where $P(A, B, C)$ represents the probability that the three vertices (A, B, C) of an up-pointing triangle are all connected, and $P(\overline{A}, \overline{B}, \overline{C})$ is the probability that none of the three vertices are connected. For this modified system consisting of one-patch disks, the method leads to that the percolation threshold is the root of equation $216\chi^3 - 756\chi^2 + 18\chi + 215 = 0$ with $\chi \in (0, 1)$, which gives $\chi_c = 0.600\,451\,160\,625\ldots$. This exact threshold can also be obtained by solving the critical polynomial $P_B(L) = R_2 - R_0 = 0$ for the smallest block with the linear size $L = 2$. Our MC calculations of $P_B(L)$ for larger L are also consistent with this value. It is expected that the modified kagome lattice consisting of disks with more patches can also be exactly solved, which we leave for future work.

In the above models, we assume that each particle is randomly rotating with its center being fixed at a vertex of the lattice. For a system in which there are interactions between patchy particles, this corresponds to the high-temperature limit of the system at full occupancy of the lattice. Since there is no correlation between different particles, the universality class of the percolation transitions is the same as ordinary percolation in two dimensions. It will be interesting to investigate the interplay of percolation and different thermodynamic phases for patchy particles at finite temperatures on lattices in two dimensions [16–18], where universal properties might be different. For example, for rigid rods of length k on the square lattice, as k changes, it was found that the percolating probability at the percolation threshold varies continuously for the anisotropic (aligned) case, while it remains the same for the isotropic case [51] (with fixed system shape and boundary conditions, since dimensionless quantities such as the percolating or wrapping probabilities depend on these factors [42–44]). On the square lattice, the self-assembled rigid rods exhibit nematic phases, for which the average length of assembled linear chains becomes longer as the temperature decreases. Thus, if there was a line of percolation transition in the ordered nematic phase, it should be expected that the percolating probability along the line changes continuously. Similar behaviors have been found in percolation of Janus disks on the triangular lattice at finite temperatures, which will be reported in the future [52]. Percolation and phase transitions of patchy particles in continuum space in two dimensions also demand more investigations [53,54].

Finally, we note that our calculation of the probabilities of different patch-covering structures of a particle implies an alternative way to define the models: the "patch-covering" structures of a particle can be regarded as discrete states of a vertex, and various states of a vertex occur with different probabilities. This transforms the continuously rotating particle model into a discrete "spin" model on the lattices, for which more efficient numerical simulations may be performed. New models are obtained if one allows the states to be different from those of the patchy particles.

ACKNOWLEDGMENTS

J.W. and H.H. thank W. Xu and Y. Deng for a previous collaboration on combining MC simulations and the critical polynomial method to study nonplanar and continuum percolation models [38]. The authors acknowledge an anonymous referee for suggesting the modification to the kagome lattice presented in the last section. This work was supported by the National Natural Science Foundation of China under Grant No. 11905001, and by the Anhui Provincial Natural Science Foundation under Grant No. 1908085QA23. We also acknowledge the High-Performance Computing Platform of Anhui University for providing computing resources.

[1] A. Walther and A. H. E. Mueller, Janus particles: Synthesis, self-assembly, physical properties, and applications, Chem. Rev. **113**, 5194 (2013).

[2] J. Zhang, B. A. Grzybowski, and S. Granick, Janus particle synthesis, assembly, and application, Langmuir **33**, 6964 (2017).

[3] F. Sciortino and E. Zaccarelli, Equilibrium gels of limited valence colloids, Curr. Opin. Colloid Interface Sci. **30**, 90 (2017).

[4] F. Smallenburg, L. Filion, and F. Sciortino, Erasing no-man's land by thermodynamically stabilizing the liquid-liquid transition in tetrahedral particles, Nat. Phys. **10**, 653 (2014).

[5] Q. Chen, S. C. Bae, and S. Granick, Directed self-assembly of a colloidal kagome lattice, Nature (London) **469**, 381 (2011).

[6] X. M. Mao, Q. Chen, and S. Granick, Entropy favours open colloidal lattices, Nat. Mater. **12**, 217 (2013).

[7] Z. W. Li, Y. W. Sun, Y. H. Wang, Y. L. Zhu, Z. Y. Lu, and Z. Y. Sun, Kinetics-controlled design principles for two-dimensional open lattices using atom-mimicking patchy particles, Nanoscale **12**, 4544 (2020).

[8] J. M. Tavares, B. Holder, and M. M. Telo da Gama, Structure and phase diagram of self-assembled rigid rods: Equilibrium polydispersity and nematic ordering in two dimensions, Phys. Rev. E **79**, 021505 (2009).

[9] L. G. López, D. H. Linares, and A. J. Ramirez-Pastor, Critical exponents and universality for the isotropic-nematic phase transition in a system of self-assembled rigid rods on a lattice, Phys. Rev. E **80**, 040105(R) (2009).

[10] N. G. Almarza, J. M. Tavares, and M. M. Telo da Gama, Effect of polydispersity on the ordering transition of adsorbed self-assembled rigid rods, Phys. Rev. E **82**, 061117 (2010).

[11] L. G. López, D. H. Linares, and A. J. Ramirez-Pastor, Comment on "Effect of polydispersity on the ordering transition of adsorbed self-assembled rigid rods," Phys. Rev. E **85**, 053101 (2012).

[12] N. G. Almarza, J. M. Tavares, and M. M. Telo da Gama, Reply to "Comment on 'Effect of polydispersity on the ordering transition of adsorbed self-assembled rigid rods,'" Phys. Rev. E **85**, 053102 (2012).

[13] L. G. López, D. H. Linares, and A. J. Ramirez-Pastor, Critical behavior of self-assembled rigid rods on triangular and honeycomb lattices, J. Chem. Phys. **133**, 134702 (2010).
[14] L. G. López, D. H. Linares, A. J. Ramirez-Pastor, and S. A. Cannas, Phase diagram of self-assembled rigid rods on two-dimensional lattices: Theory and Monte Carlo simulations, J. Chem. Phys. **133**, 134706 (2010).
[15] N. G. Almarza, J. M. Tavares, and M. M. Telo da Gama, Communication: The criticality of self-assembled rigid rods on triangular lattices, J. Chem. Phys. **134**, 071101 (2011).
[16] K. Mitsumoto and H. Yoshino, Orientational ordering of closely packed Janus particles, Soft Matter **14**, 3919 (2018).
[17] A. Patrykiejew and W. Rżysko, Order-disorder transitions in systems of Janus-like particles on a triangular lattice, Physica A **548**, 123883 (2020).
[18] A. Patrykiejew and W. Rżysko, Two-dimensional Janus-like particles on a triangular lattice, Soft Matter **16**, 6633 (2020).
[19] D. Stauffer and A. Aharony, *Introduction to Percolation Theory*, 2nd ed. (Taylor & Francis, London, 1994).
[20] A. A. Saberi, Recent advances in percolation theory and its applications, Phys. Rep. **578**, 1 (2015).
[21] F. Seiferling, D. de las Heras, and M. M. Telo da Gama, Percolation in binary and ternary mixtures of patchy colloids, J. Chem. Phys. **145**, 074903 (2016).
[22] J. L. B. de Araújo, F. F. Munarin, G. A. Farias, F. M. Peeters, and W. P. Ferreira, Structure and reentrant percolation in an inverse patchy colloidal system, Phys. Rev. E **95**, 062606 (2017).
[23] L. L. Treffenstädt, N. A. M. Araújo, and D. de las Heras, Percolation of functionalized colloids on patterned substrates, Soft Matter **14**, 3572 (2018).
[24] G. Wang and J. W. Swan, Surface heterogeneity affects percolation and gelation of colloids: Dynamic simulations with random patchy spheres, Soft Matter **15**, 5094 (2019).
[25] J. Song, M. H. Rizvi, B. B. Lynch, J. Ilavsky, D. Mankus, J. B. Tracy, G. H. McKinley, and N. Holten-Andersen, Programmable anisotropy and percolation in supramolecular patchy particle gels, ACS Nano **14**, 17018 (2020).
[26] M. J. Kartha and A. G. Banpurkar, Why patchy diffusion-limited aggregation belongs to the directed-percolation universality class, Phys. Rev. E **94**, 062108 (2016).
[27] S. A. Safran, I. Webman, and G. S. Grest, Percolation in interacting colloids, Phys. Rev. A **32**, 506 (1985).
[28] A. Hasmy, S. Ispas, and B. Hehlen, Percolation transitions in compressed SiO_2 glasses, Nature (London) **599**, 62 (2021).
[29] C. R. Scullard and R. M. Ziff, Critical Surfaces for General Bond Percolation Problems, Phys. Rev. Lett. **100**, 185701 (2008).
[30] C. R. Scullard and R. M. Ziff, Critical surfaces for general inhomogeneous bond percolation problems, J. Stat. Mech. (2010) P03021.
[31] C. R. Scullard, Polynomial sequences for bond percolation critical thresholds, J. Stat. Mech. (2011) P09022.
[32] C. R. Scullard, Percolation critical polynomials as a graph invariant, Phys. Rev. E **86**, 041131 (2012).
[33] C. R. Scullard and J. L. Jacobsen, Transfer matrix computation of generalized critical polynomials in percolation, J. Phys. A: Math. Theor. **45**, 494004 (2012).
[34] J. L. Jacobsen, High-precision percolation thresholds and Potts-model critical manifolds from graph polynomials, J. Phys. A: Math. Theor. **47**, 135001 (2014).
[35] J. L. Jacobsen, Critical points of Potts and O(N) models from eigenvalue identities in periodic Temperley-Lieb algebras, J. Phys. A: Math. Theor. **48**, 454003 (2015).
[36] C. R. Scullard and J. L. Jacobsen, Potts-model critical manifolds revisited, J. Phys. A: Math. Theor. **49**, 125003 (2016).
[37] C. R. Scullard and J. L. Jacobsen, Bond percolation thresholds on Archimedean lattices from critical polynomial roots, Phys. Rev. Res. **2**, 012050(R) (2020).
[38] W. H. Xu, J. F. Wang, H. Hu, and Y. J. Deng, Critical polynomials in the nonplanar and continuum percolation models, Phys. Rev. E **103**, 022127 (2021).
[39] B. Grünbaum and G. C. Shephard, *Tillings and Patterns* (Freeman, New York, 1987).
[40] P. N. Suding and R. M. Ziff, Site percolation thresholds for Archimedean lattices, Phys. Rev. E **60**, 275 (1999).
[41] See Supplemental Material at http://link.aps.org/supplemental/10.1103/PhysRevE.105.034118 for the following (1) Further simulation details. (2) More plots for estimating the thresholds values. (3) Calculations for one-patch disks on the frieze lattice. (4) Calculations for disks with an arbitrary number of patches. (5) Demonstration for symmetries between n-patch disks with mod $(n, n_0) = m$ and $n_0 - m$.
[42] R. P. Langlands, C. Pichet, Ph. Pouliot, and Y. Saint-Aubin, On the universality of crossing probabilities in two-dimensional percolation, J. Stat. Phys. **67**, 553 (1992).
[43] H. T. Pinson, Critical percolation on the torus, J. Stat. Phys. **75**, 1167 (1994).
[44] R. M. Ziff, C. D. Lorenz, and P. Kleban, Shape-dependent universality in percolation, Physica A **266**, 17 (1999).
[45] M. P. Nightingale, Phenomenological renormalization and finite-size scaling, in *Finite-Size Scaling and Numerical Simulation of Statistical Systems*, edited by V. Privman (World Scientific, Singapore, 1990), pp. 307–314.
[46] M. F. Sykes and J. W. Essam, Exact critical percolation probabilities for site and bond problems in two dimensions, J. Math. Phys. **5**, 1117 (1964).
[47] W. S. Oliveira, J. P. de Lima, N. C. Costa, and R. R. dos Santos, Percolation on Lieb lattices, Phys. Rev. E **104**, 064122 (2021).
[48] M. Yanuka and R. Englman, Bond-site percolation: Empirical representation of critical probabilities, J. Phys. A: Math. Gen. **23**, L339 (1990).
[49] Y. Y. Tarasevich and S. van der Marck, An investigation of site-bond percolation on many lattices, Int. J. Mod. Phys. C **10**, 1193 (1999).
[50] R. M. Ziff, Generalized cell-dual-cell transformation and exact thresholds for percolation, Phys. Rev. E **73**, 016134 (2006).
[51] P. Longone, P. M. Centres, and A. J. Ramirez-Pastor, Percolation of aligned rigid rods on two-dimensional square lattices, Phys. Rev. E **85**, 011108 (2012).
[52] H. Hu and X. Zhang (unpublished).
[53] T. Huang, Y. Han, and Y. Chen, Melting and solid-solid transitions of two-dimensional crystals composed of Janus spheres, Soft Matter **16**, 3015 (2020).
[54] Y. H. Liang, B. Ma, and M. O. de la Cruz, Reverse order-disorder transition of Janus particles confined in two dimensions, Phys. Rev. E **103**, 062607 (2021).

Correction: The first affiliation contained an error and has been fixed.